interpret by pathologists.[2] Among them, diagnosis of MFH has been the most controversial issue.[3–5] MFH has been considered the most common soft tissue sarcoma of adults; it is manifested by a broad range of histological appearances and consists of four subtypes: storiform and pleomorphic type, myxoid type, giant cell type and inflammatory type. Recent clinicopathological, ultrastructural and immunohistochemical studies revealed that MFH shows no evidence of true histiocytic differentiation and that it is not a single entity but rather a heterogeneous collection of pleomorphic subtypes of other sarcomas. Since each type of sarcoma other than MFH shows distinct biological behavior, particularly in local recurrence or metastasis rate, MFH showing a variety of clinicopathological characteristics should be further reclassified to correctly evaluate the malignant potential of each case. In the latest edition of the WHO classification, myxoid type MFH was classified as myxofibrosarcoma in the fibroblastic category, and other subtypes of MFH without any evidence of differentiation were classified as undifferentiated high grade pleomorphic sarcoma.[6] WHO classification also suggested that the term 'MFH' might disappear when criteria for the diagnosis of pleomorphic sarcomas showing a distinct differentiation state can be reproducibly defined.[6] In this work, we used the term 'MFH' to identify tumors diagnosed as storiform and pleomorphic type MFH, and the term 'myxofibrosarcoma' for so-called MFH with predominant (>50%) myxoid features conventionally diagnosed as myxoid type MFH.

Recently, several studies report gene expression profiling of soft tissue tumors using microarray technologies to provide new insights into the tumor characterization. They described distinct patterns of gene expression in respective tumors with single, recurrent genetic aberrations, such as synovial sarcoma, myxoid/round cell liposarcoma, clear cell sarcoma or gastrointestinal stromal tumors, and heterogeneous patterns in spindle cell and pleomorphic sarcomas which are generally characterized by complex chromosomal aberrations.[7–12] No further detailed analysis of gene expression in spindle cell and pleomorphic sarcomas have been reported so far.

In this study, we analyzed gene expression profile of total 105 cases representing 10 types of soft tissue tumors to identify their molecular characteristics. We observed similarity in gene expression among spindle cell and pleomorphic sarcomas, forming a relatively loose cluster, which is separated from the distinct clusters of synovial sarcoma, myxoid/round cell liposarcoma and lipoma + well-differentiated liposarcoma. Next, we primarily analyzed 64 samples of spindle cell and pleomorphic sarcomas and showed heterogeneity of MFH in terms of gene expression. We selected genes that could clearly distinguish between dedifferentiated liposarcoma, myxofibrosarcoma, leiomyosarcoma, malignant peripheral nerve sheath tumor (MPNST) and fibrosarcoma and quantified similarities as distances between MFH samples and the five sarcoma types.

Materials and methods

Patients and Tumor Samples

Characteristics of 105 soft tissue tumors used in this study are shown in Supplementary data 1. Among them, 35 samples were previously analyzed in a different method.[13] All patients received histological diagnosis of primary soft tissue tumor at National Cancer Center Hospital, Tokyo, from 1996 to 2002. In this paper, we use the term 'MFH' to describe samples diagnosed as storiform and pleomorphic type MFH showing predominant pleomorphic features without immunohistochemical phenotypes characteristic of specific differentiation, and the term 'myxofibrosarcoma' to describe MFH with predominant (>50%) myxoid features conventionally diagnosed as myxoid type MFH. Before the gene expression analysis pathologists confirmed the diagnosis of MFH was appropriate at the time of primary diagnosis. Tumor samples were collected from the part with macroscopically high tumor content by pathologists immediately after surgical excision and cryopreserved in liquid nitrogen until use. This study was approved by the ethics committee of National Cancer Center and conducted according to tenets of the Declaration of Helsinki.

Gene Expression Profiling

Total RNA was isolated using TRIzol (Invitrogen, Carlsbad, CA, USA) according to the manufacturer's instruction. Samples were analyzed with a GeneChip Human Genome U133A array (Affymetrix, Santa Clara, CA, USA) containing 22 283 probe sets. Target cRNA preparation from total RNA, hybridization to the microarray, washing and staining with an antibody amplification procedure and scanning were all carried out according to the manufacturer's instructions. The expression value (Signal) of each probe set was calculated using GeneChip Operating Software (GCOS) ver. 1.3 (Affymetrix), so that the mean of expression values in each experiment was set at 100 to adjust for minor differences between experiments.

Statistical Analysis

Gene expression data were subsequently imported into GeneSpring GX7.2 software (Agilent Technologies, Santa Clara, CA, USA) and normalized to the median of all samples enrolled in the analysis and log-transformed for each gene. Hierarchical clustering analysis was performed using Pearson's correlation. To select appropriate probe sets defining five

types of spindle cell and pleomorphic sarcomas (dedifferentiated liposarcoma, myxofibrosarcoma, leiomyosarcoma, MPNST and fibrosarcoma), we performed Student's *t*-tests between one and the other four sarcoma types. The top 50 probe sets with low *P*-values in each *t*-test were summed. The centroid of each sarcoma type was determined by calculating the average of the selected probe sets. The distance (D) from a centroid to a sample was defined as $D=1-r$, using Pearson's correlation coefficient (r, $-1 \leq r \leq 1$). Inter-centroid distances were also calculated using Pearson's correlation coefficient.

Histological Analysis

Histological sections of the tumors were stained with hematoxylin and eosin and reviewed for all samples, and representative sections were examined immunohistochemically using the labeled streptavidin–biotin method. Sections were dewaxed, rehydrated and moistened with phosphate-buffered saline (pH 7.4), autoclaved at 121°C for 10 min in 10 mM citrate buffer (pH 6.0) and incubated with antibodies to the following molecules on an automated immunostaining system i6000 (BioGenex, San Ramon, CA, USA) for 30 min, as described previously:[14] vimentin, desmin, α-smooth muscle actin (αSMA), muscle-specific actin, h-caldesmon, CD34, S-100 protein, epithelial membrane antigen, cytokeratin and neurofilament. Heat-induced epitope retrieval was not undertaken when sections were stained with antibodies to S-100 protein and epithelial membrane antigen.

Quantitative RT-PCR

Real-time quantitative reverse transcription (RT)-PCR was carried out using the 7500 Fast Real-Time PCR System (Applied Biosystems, Foster City, CA, USA) with FastStart TaqMan Probe Master (Rox) and Universal ProbeLibrary (Roche Applied Science, Mannheim, Germany). One microgram of total RNA from 17 tumor samples (myxofibrosarcoma ($n=5$), MFH ($n=7$), leiomyosarcoma ($n=2$) and MPNST ($n=3$)) was reverse-transcribed to synthesize single-stranded cDNAs using SuperScript III (Invitrogen), and 1/100 of the cDNA was used for each PCR. Probes and primers were designed using Probe Finder software (Roche Applied Science) (Supplementary data 2). Transcript levels were normalized to that of the *ACTB* transcript.

Results

Overview of Gene Expression in Soft Tissue Sarcomas

Gene expression data of 105 soft tissue tumor samples consisting of synovial sarcoma ($n=16$), myxoid/round cell liposarcoma ($n=19$), lipoma ($n=3$), well-differentiated liposarcoma ($n=3$), dedifferentiated liposarcoma ($n=15$), myxofibrosarcoma ($n=15$), leiomyosarcoma ($n=6$), MPNST ($n=3$), fibrosarcoma ($n=4$) and MFH ($n=21$) were obtained using an oligonucleotide microarray containing 22 283 probe sets. Among them, 12 599 probe sets whose expression values were not less than 100 in at least 3 of 105 samples were analyzed. To overview the transcriptome of sarcomas in our data set, we first performed principal component analysis with 12 599 probe sets (Figure 1a), which is a decomposition technique to reduce multidimensional data into several specialized dimensions. The x and y axes in Figure 1a indicate the first and second principal components, respectively, representing the top and second largest fractions of the overall variability. In this analysis, 105 samples were roughly classified into four groups based on their position relative to the first and second principal components. Both synovial sarcoma and myxoid/round cell liposarcoma samples were located on the negative side of the first principal component, while well-differentiated liposarcoma, dedifferentiated liposarcoma and other spindle cell and pleomorphic sarcoma samples were on the positive side. On the negative side of the second principal component were myxoid/round cell liposarcoma, well-differentiated liposarcoma and lipoma samples, all of which are adipocytic tumors. Interestingly, some dedifferentiated liposarcoma samples were distributed close to well-differentiated liposarcoma samples, while others were midway between well-differentiated liposarcoma and other spindle cell and pleomorphic sarcoma samples. These results suggest that the first principal component was associated with the difference between synovial sarcoma + myxoid/round cell liposarcoma and spindle cell and pleomorphic sarcomas, and that the second principal component was associated with adipocytic differentiation. Probe sets contributing significantly to the first and second principal components are listed in Supplementary data 3.

To identify genes whose expression differed in a statistically significant manner among all sarcoma types, we performed an analysis of variance (ANOVA) among 10 tumor types and selected 2590 probe sets with *P*-values of less than 1.0×10^{-5}. Two-dimensional hierarchical clustering analysis using those 2590 probe sets showed that synovial sarcoma and myxoid/round cell liposarcoma samples displayed distinct gene expression profiles and formed robust clusters (Figure 1b). On the other hand, myxofibrosarcoma, leiomyosarcoma, MPNST, fibrosarcoma and MFH samples did not show distinct gene expression profiles, but rather formed a single loose cluster and shared a similar expression profile. We also found that lipoma and well-differentiated liposarcoma samples and some of the dedifferentiated liposarcoma samples displayed similar gene expression profiles and formed a cluster, whereas

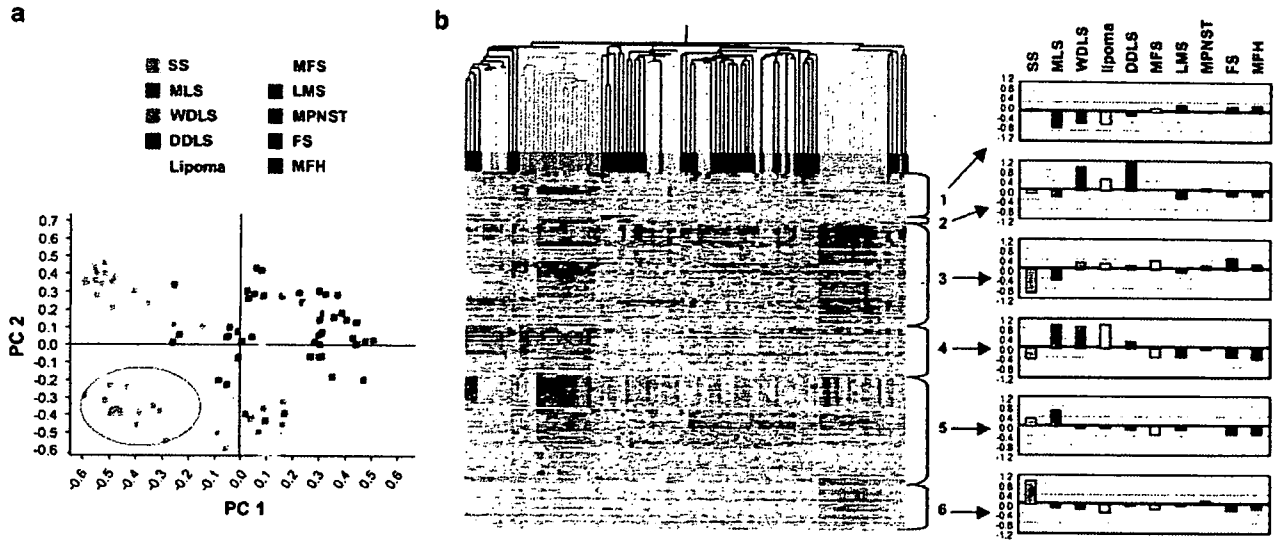

Figure 1 Gene expression overview of 105 soft tissue tumors. (a) Principal component analysis. A total of 12599 probe sets with expression values not less than 100 in at least three samples were used in this analysis. *x* and *y* axes represent the first and second principal components (PC1 and PC2), respectively. Each dot represents a sample colored by its histological type. (**b**) Two-dimensional hierarchical clustering analysis. A total of 2590 probe sets differentially expressed among histological types ($P<1.0\times10^{-5}$ by ANOVA) were used. Columns represent samples and rows represent probe sets. Red and green indicate high and low expression, respectively. The 2590 probe sets were roughly divided into six clusters (clusters 1–6). The six graphs on the right show averages of normalized expression values of those clusters for each histological type. Note that spindle cell and pleomorphic sarcomas, such as dedifferentiated liposarcoma, myxofibrosarcoma, leiomyosarcoma, MPNST, fibrosarcoma and MFH, form a loose cluster and share a similar expression profile compared with synovial sarcoma, myxoid/round cell liposarcoma, well-differentiated liposarcoma and lipoma. SS, synovial sarcoma; MLS, myxoid/round cell liposarcoma; WDLS, well-differentiated liposarcoma; DDLS, dedifferentiated liposarcoma; MFS, myxofibrosarcoma; LMS, leiomyosarcoma and FS, fibrosarcoma.

the other dedifferentiated liposarcoma samples did not share that profile but instead formed a loose cluster with fibrosarcoma, myxofibrosarcoma and MFH samples.

The 2590 probe sets were classified into six clusters according to their expression patterns (Figure 1b and Supplementary data 4). Interestingly, we found two major clusters (clusters 3 and 5) whose expression patterns were similar between synovial sarcoma and myxoid/round cell liposarcoma samples. Cluster 3, whose expression was low in synovial sarcoma and myxoid/round cell liposarcoma, contained many HLA genes, and cluster 5, whose expression was high in both synovial sarcoma and myxoid/round cell liposarcoma, contained many genes encoding ribosomal proteins and cancer testis antigens, such as *CTAG1B*, *CTAG2* and *PRAME*. Of note, these genes contributed largely to the first principal component (see Supplementary data 3). On the other hand, cluster 1, whose expression was low in myxoid/round cell liposarcoma, well-differentiated liposarcoma and lipoma samples, included cell cycle associated genes such as *CCNB1*, *CDKN3*, and *CDC20*, while cluster 4, whose expression was high in myxoid/round cell liposarcoma, well-differentiated liposarcoma and lipoma samples, included adipocytic differentiation-associated genes such as *LPL*, *ACACB* and *PLIN*. These genes contributed largely to the second principal component (see Supplementary data 3). Cluster 6, whose expression was high in synovial sarcoma, included *COL2A1*, *COL9A3*, *SSX1* and *SSX2*. The small but robust cluster, cluster 2, consisted of *MDM2*, *CDK4* and other genes located in 12q13-15, which are known to be amplified in both well-differentiated liposarcoma and dedifferentiated liposarcoma.

Heterogeneity of MFH in Gene Expression and Classification of Spindle Cell and Pleomorphic Sarcomas

Spindle cell and pleomorphic sarcomas frequently display overlapping histological appearance and immunohistochemical phenotypes. Samples from these types of sarcoma did not separate into distinct histological types in the analysis using whole samples (Figure 1). To determine whether they could be grouped by gene expression, we analyzed 64 samples of spindle cell and pleomorphic sarcomas (dedifferentiated liposarcoma, myxofibrosarcoma, leiomyosarcoma, MPNST, fibrosarcoma and MFH). We performed principal component analysis with 11300 probe sets whose expression values were not less than 100 in at least three of 64 samples, and two-dimensional hierarchical clustering analysis using 1671 probe sets selected by ANOVA among six sarcoma types ($P<0.01$) (Supplementary data 5). In the clustering analysis,

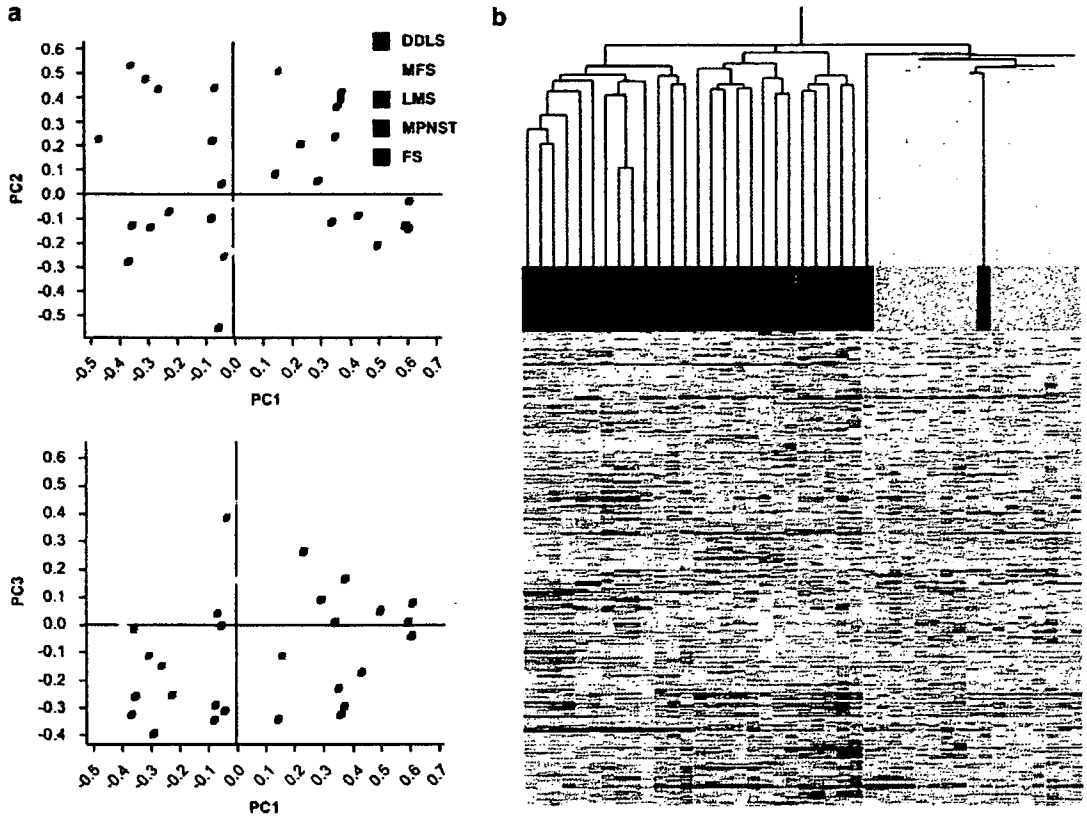

Figure 2 Classification of spindle cell and pleomorphic sarcomas without MFH. (**a**) Principal component analysis. A total of 11 300 probe sets with expression values not less than 100 in at least three of 64 spindle cell and pleomorphic sarcoma samples including MFH were used in this analysis. *x* and *y* axes in the upper panel represent the first and second principal components (PC1 and PC2), and *x* and *y* axes in the lower panel represent the first and third principal components (PC1 and PC3), respectively. (**b**) Two-dimensional hierarchical clustering analysis. A total of 1457 probe sets differentially expressed among five types of spindle cell and pleomorphic sarcomas ($P<0.01$ by ANOVA) were used. Columns represent samples and rows represent probe sets. Red and green indicate high and low expression, respectively. Note that most samples formed clusters corresponding to their histology. DDLS, dedifferentiated liposarcoma; MFS, myxofibrosarcoma; LMS, leiomyosarcoma and FS, fibrosarcoma.

dedifferentiated liposarcoma, myxofibrosarcoma, leiomyosarcoma, MPNST and fibrosarcoma samples appeared to form their own clusters, whereas those of MFH partitioned into several groups, some close to clusters of other sarcomas. These results suggest that MFH is heterogeneous in terms of gene expression as observed histologically.

Next, we analyzed 43 samples of five spindle cell and pleomorphic sarcomas (dedifferentiated liposarcoma, myxofibrosarcoma, leiomyosarcoma, MPNST and fibrosarcoma) and excluded MFH samples. In principal component analysis with 11 300 probe sets, samples of the same tumor type appeared to cluster (Figure 2a). We then performed two-dimensional hierarchical clustering analysis with 1457 probe sets selected from the 11 300 probe sets by ANOVA among five sarcoma types ($P<0.01$) (Figure 2b). Although we found three exceptions (one leiomyosarcoma and two dedifferentiated liposarcoma samples), almost all dedifferentiated liposarcoma, myxofibrosarcoma, leiomyosarcoma, MPNST and fibrosarcoma samples formed their own respective clusters suggesting that each type of spindle cell and pleomorphic sarcoma formed a homogeneous group in terms of gene expression by excluding MFH samples.

Distances of MFH Samples from Other Spindle Cell and Pleomorphic Sarcomas

Since MFH samples did not form a clearly distinctive cluster, we next addressed a question whether MFH could be reclassified into other types of spindle cell and pleomorphic sarcomas by gene expression and quantified similarities between MFH samples and those sarcoma types using differentially expressed genes. To select appropriate probe sets defining spindle cell and pleomorphic sarcomas, we performed the Student's *t*-test between one and the other four of the five sarcoma types, namely, dedifferentiated liposarcoma, myxofibrosarcoma, leiomyosarcoma, MPNST and fibrosarcoma. In this analysis, we excluded three exceptional samples

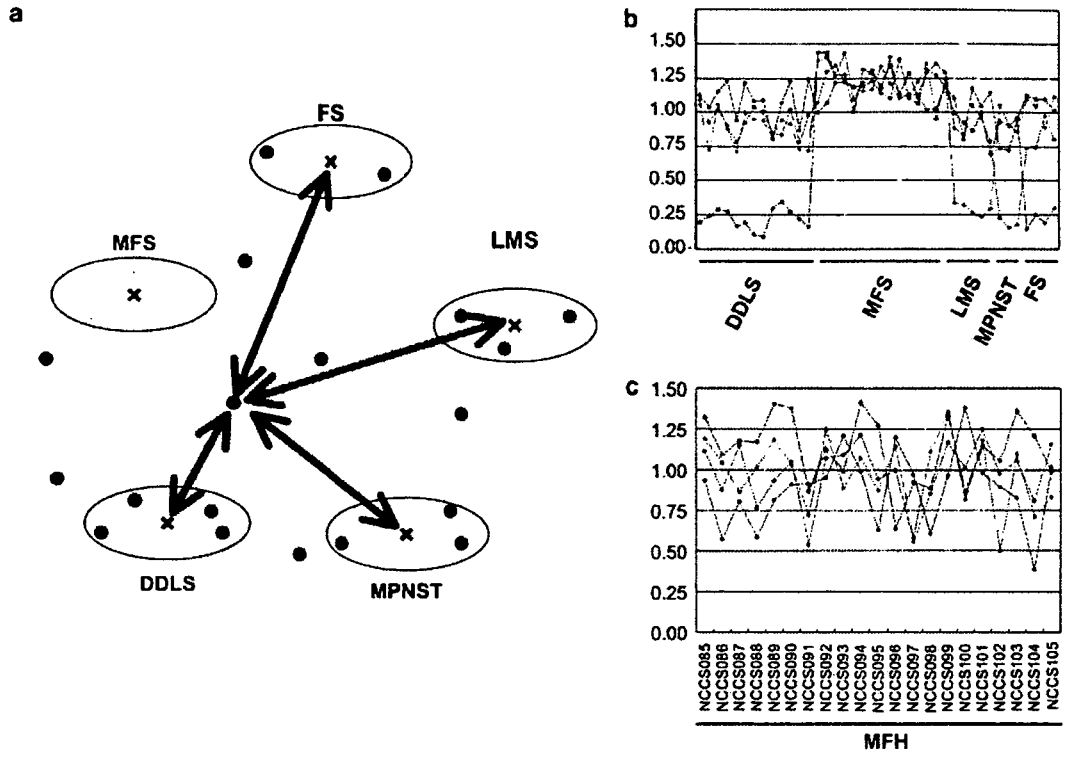

Figure 3 Distance evaluation of spindle cell and pleomorphic sarcoma samples from five sarcoma types. (**a**) Scheme of distance calculation. Each dot represents a sample colored according to its histology. Each × -mark represents the centroid of each histological type of sarcoma. Each arrow indicates the distance from a sample to a centroid colored by the histology. (**b**) Distances of 40 control samples from the five centroids. Note that the closest centroids matched their histology. (**c**) Distances of 21 MFH samples from the five centroids. DDLS, dedifferentiated liposarcoma; MFS, myxofibrosarcoma; LMS, leiomyosarcoma and FS, fibrosarcoma.

that did not fall into the appropriate cluster (Figure 2b). The top 50 probe sets with low *P*-values in each *t*-test were summed to obtain 248 probe sets (Supplementary data 6). On the basis of the expression of these 248 probe sets, the centroids of those five sarcoma types were calculated in advance, and inter-centroid distances and distances from five centroids to each control sample ($n=40$) were evaluated (Supplementary data 7 and Figure 3a and b). All inter-centroid distances were greater than 0.77 and the closest centroids for 40 control samples matched their histological types (Figure 3b), indicating that the evaluated distances were good indicators of sarcoma classification. We then evaluated the distances of each MFH sample from the five centroids (Figure 3c) and focused on determining the minimum (D_{min}) of the five distances. Small D_{min} values indicate high similarity to one of the five histological types in terms of gene expression. We used two cutoff values of 0.5 and 0.75 to evaluate similarity, because the majority of D_{min} values in control samples were less than 0.5 and most of the remaining four distances in each control sample were greater than 0.75. Among 21 samples, 3 showed marked similarity ($D_{min} \leq 0.5$), 12 showed moderate similarity ($0.5 < D_{min} \leq 0.75$) and the remaining 6 showed little similarity ($D_{min} > 0.75$). Among 15 MFH samples showing high or moderate similarity ($D_{min} \leq 0.75$), 6 were similar to myxofibrosarcoma, 5 to fibrosarcoma, 2 to MPNST and 1 each to dedifferentiated liposarcoma and leiomyosarcoma.

Histological Reviews

We re-examined the histology of 21 MFH samples with the knowledge of similarity to other types of spindle cell and pleomorphic sarcomas based on gene expression. Three MFH samples that showed high gene expression similarity ($D_{min} \leq 0.5$) displayed marked pleomorphism, indicating that a diagnosis of MFH was appropriate at the time of diagnosis. However, these samples also showed histological signatures of relevant subtypes. The NCCS099 sample, which was significantly close to the myxofibrosarcoma centroid ($D_{min} = 0.46$), showed prominent myxoid features very similar to myxofibrosarcoma in one third of the tumor (Figure 4a). The NCCS102 sample which was very close to the leiomyosarcoma centroid ($D_{min} = 0.50$) was positive for desmin and αSMA (Figure 4b–d). The NCCS104 sample, which was very close to the fibrosarcoma centroid ($D_{min} = 0.39$), showed focal

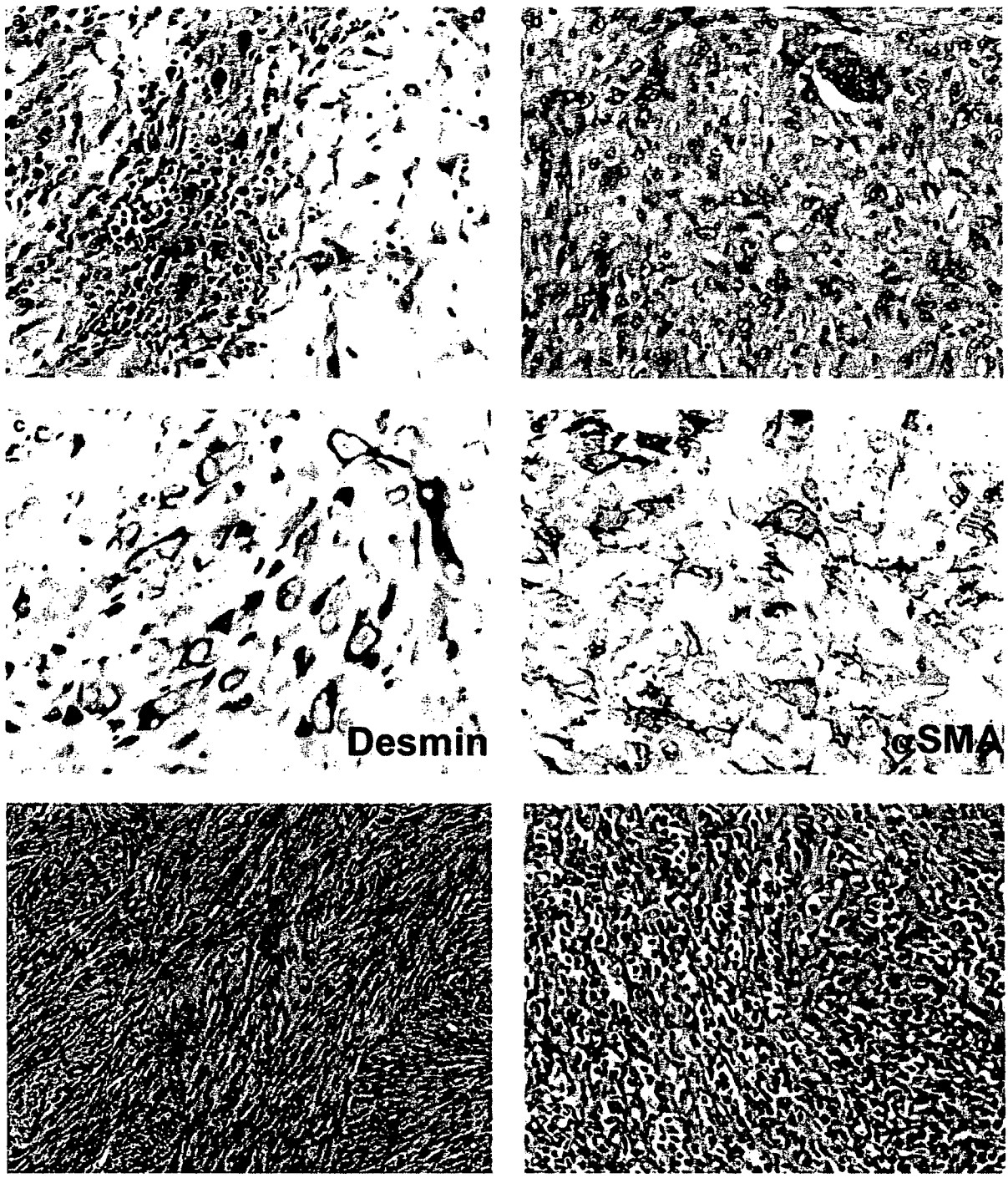

Figure 4 Histological review. (**a**) The border between pleomorphic area and myxoid area observed in the NCCS099 sample ($D_{min} = 0.46$ to myxofibrosarcoma) (hematoxylin and eosin stain). (**b–d**) Histology of the NCCS102 sample ($D_{min} = 0.50$ to leiomyosarcoma). This tumor showed marked pleomorphism (**b**) hematoxylin and eosin stain, but tumor cells were positive for desmin (**c**) and αSMA (**d**). (**e**) Fibrosarcomatous fascicular area seen in the NCCS104 sample ($D_{min} = 0.39$ to fibrosarcoma) (hematoxylin and eosin stain). (**f**) Epithelioid structure observed in the NCCS097 sample ($D_{min} = 0.56$ to MPNST) (hematoxylin and eosin stain).

fibrosarcoma-like herringbone and fascicular patterns by microscopic analysis (Figure 4e).

Among twelve samples showing moderate similarity to other types of sarcomas ($0.50 < D_{min} \leq 0.75$), the NCCS096 sample close to the dedifferentiated liposarcoma centroid ($D_{min} = 0.64$) was obtained from a recurrent sarcoma in the retroperitoneum. Although microscopic findings did not show

evidence of adipocytic differentiation or features of well-differentiated liposarcoma in regions adjacent to the tumor, the site of involvement suggested the possibility that the tumor originated from dedifferentiated liposarcoma. All five samples close to myxofibrosarcoma ($0.50 < D_{min} \leq 0.75$) showed scattered myxoid areas, but these findings were not sufficient to reclassify them as myxofibrosarcoma histologically. The NCCS097 sample, another pleomorphic sarcoma close to the MPNST centroid ($D_{min} = 0.56$), exhibited scattered whorled and epithelioid structures (Figure 4f) as well as tumor cells positive for cytokeratin, neurofilament and αSMA, indicating that this tumor had neuroectodermal differentiation. Its similarity to leiomyosarcoma ($D = 0.58$) would be reflected in αSMA positivity. For the NCCS091 sample close to MPNST and the other four close to fibrosarcoma, we did not observe any significant histological similarity to MPNST or fibrosarcoma, respectively. In summary, although more than half of the MFH samples ($n = 12$) were moderately similar in terms of gene expression to other sarcomas ($0.50 < D_{min} \leq 0.75$), only little resemblance was detectable by histological examination. Finally, the remaining six samples with high D_{min} values ($D_{min} > 0.75$) showed no identifiable histological similarity to the five sarcoma types (dedifferentiated liposarcoma, myxoid/round cell liposarcoma, leiomyosarcoma, MPNST and fibrosarcoma).

Genes Overexpressed in Myxofibrosarcoma

Diagnostically useful markers for myxofibrosarcoma are not well known. To search for candidate markers that genetically characterize myxofibrosarcoma, we selected upregulated genes by comparing myxofibrosarcoma samples ($n = 15$) with other spindle cell and pleomorphic sarcoma samples ($n = 25$). Three samples excluded from the previous analysis and 21 samples of MFH were not used for the marker search. From 11 300 probe sets, we selected 10 probe sets (five genes) with *P*-values < 0.001 based on the Student's *t*-test and more than five-fold greater expression (Table 1). Among them, expression of four probe sets (four genes) in respective spindle cell and pleomorphic sarcomas are shown in Figure 5a by the box-and-whisker plots. Since *ANK1* expression in MFH was much higher than that seen in myxofibrosarcoma (data not shown), its upregulation was not considered to be specific to myxofibrosarcoma. We performed quantitative RT-PCR with three other genes, *WISP2*, *GPR64* and *TNXB*, to verify the microarray findings (Figure 5b). Quantitative RT-PCR data confirmed consistent high expression of *GPR64* and *TNXB* in myxofibrosarcoma samples and in some MFH samples showing similarity to myxofibrosarcoma in terms of gene expression.

Discussion

An important aim of this study was to obtain new insights to classify a diverse group of soft tissue sarcomas. Our data showed that soft tissue sarcomas examined roughly fell into four groups (Figure 1a) (1) synovial sarcoma; (2) myxoid/round cell liposarcoma; (3) lipoma, well-differentiated liposarcoma with part of dedifferentiated liposarcoma and (4) spindle cell and pleomorphic sarcomas. Six histological types of spindle cell and pleomorphic sarcomas (dedifferentiated liposarcoma, myxofibrosarcoma, leiomyosarcoma, MPNST, fibrosarcoma and MFH) did not display distinct profiles but they shared a similar gene expression profile, forming a loose cluster in the hierarchical clustering analysis (Figure 1b). These results were broadly consistent with previous reports,[7,10] and histological similarity among spindle cell and pleomorphic sarcomas could be explained by similarities in gene expression. We could find some MPNST samples were located adjacent to the robust synovial sarcoma cluster in the hierarchical clustering analysis (Figure 1b), indicating that those MPNST samples shared similar expression patterns with synovial sarcoma as reported by Nagayama *et al*.[8] Our data also showed a common gene expression signature in synovial sarcoma and myxoid/round cell liposarco-

Table 1 Genes highly expressed in myxofibrosarcoma

Gene symbol	*Fold change*	*P-value*	*Description*	*Probe set ID*
WISP2	10.99	1.6×10^{-5}	WNT1 inducible signaling pathway protein 2	205792_at
GPR64	10.56	7.7×10^{-5}	G protein-coupled receptor 64	206002_at
TNXB	8.30	3.7×10^{-5}	Tenascin XB	208609_s_at
ANK1	7.03	1.8×10^{-5}	Ankyrin 1, erythrocytic	208352_x_at
S100A3	6.41	3.0×10^{-7}	S100 calcium binding protein A3	206027_at
ANK1	5.99	5.5×10^{-5}	Ankyrin 1, erythrocytic	205391_x_at
TNXB	5.96	2.9×10^{-5}	Tenascin XB	213451_x_at
TNXB	5.86	6.5×10^{-4}	Tenascin XB	216339_s_at
TNXB	5.74	1.3×10^{-4}	Tenascin XB	206093_x_at
TNXB	5.74	4.7×10^{-5}	Tenascin XB	216333_x_at

The top 10 probe sets with high fold changes were selected from 321 probe sets differentially expressed ($P < 0.001$ by Student's *t*-test) between myxofibrosarcoma samples ($n = 15$) and other spindle cell and pleomorphic sarcoma samples ($n = 25$) analyzed in Figure 3b.

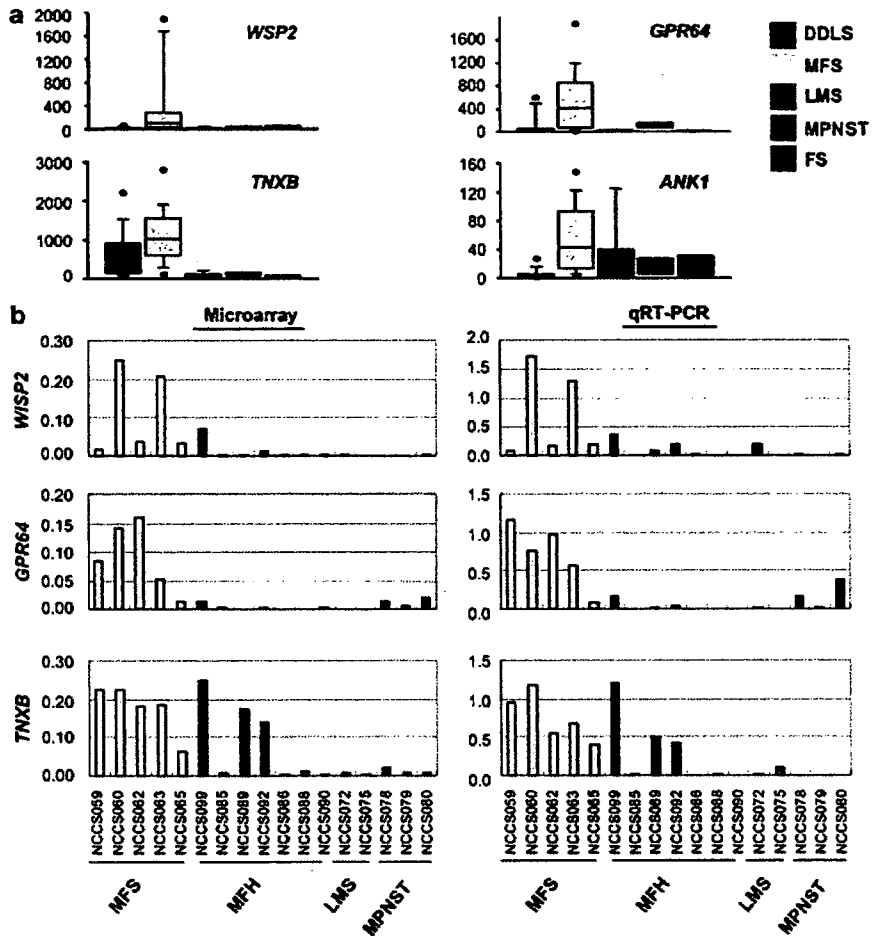

Figure 5 Genes highly expressed in myxofibrosarcoma. (**a**) Box-and-whisker plots indicating expression values for each histological type of spindle cell and pleomorphic sarcomas. A total of 40 control samples were analyzed. (**b**) Comparison between microarray analysis and quantitative RT-PCR of *WISP2*, *GPR64* and *TNXB* expression. Expression levels were normalized to that of *ACTB* in both microarray and RT-PCR data. NCCS099 ($D_{min} = 0.46$), NCCS085 ($D_{min} = 0.66$), NCCS089 ($D_{min} = 0.75$) and NCCS092 ($D_{min} = 0.66$) were similar to myxofibrosarcoma in terms of gene expression (see Figure 3c). DDLS, dedifferentiated liposarcoma; MFS, myxofibrosarcoma; LMS, leiomyosarcoma and FS, fibrosarcoma.

ma samples, distinguishing them from other tumors. Overexpression of genes encoding ribosomal proteins in myxoid/round cell liposarcoma was reported previously.[11] Another report showed that *SOX11*, *CTAG1*, *CTAG2* and *PRAME* were overexpressed in liposarcomas and absent or minimally expressed in all other tumors examined.[15] Among those genes, *CTAG1* and *PRAME* are both categorized as cancer testis antigens, and their expression in synovial sarcoma has also been reported.[16] Consistent with those reports, we found that *SOX11*, *CTAG1*, *CTAG2* and *PRAME* are highly expressed in both synovial sarcoma and myxoid/round cell liposarcoma. These similarities in gene expression may correlate with biological characteristics of synovial sarcoma and myxoid/round cell liposarcoma and suggest that these two sarcomas may share a common oncogenic pathway.

The so-called MFH was thought to be the most common soft tissue sarcoma in adults, and currently, it is widely accepted as a common morphological manifestation of a variety of poorly differentiated sarcomas. Re-evaluation of 'MFH' by different methods has been undertaken. Fletcher *et al*[5] reclassified 100 tumors primarily diagnosed as 'MFH' by histological methods and showed that the most common diagnosis was myxofibrosarcoma ($n = 29$), followed by leiomyosarcoma ($n = 20$). Hasegawa *et al*[14] examined immunoreactivity for smooth muscle markers from 100 samples of 'MFH' and reported that a large subset showed poorly differentiated smooth muscle or myofibroblastic features and should be regarded as pleomorphic leiomyosarcoma or pleomorphic myofibrosarcomas. Using comparative genomic hybridization, Derre *et al*[17] showed similar recurrent genomic imbalances in 'MFH' and leiomyosarcoma, and Coindre *et al*[18] reported that most inflammatory types of MFH developing in the retroperitoneum are identical to dedifferentiated liposarcoma. Here, we discussed

the possibility that 21 MFH samples could be reclassified into other types of spindle cell and pleomorphic sarcomas based on similarities in gene expression. For convenience of evaluation, we separated MFH samples into three groups according to the level of similarity to other sarcoma types. MFH with marked similarity ($D_{min} \leq 0.5$), MFH with moderate similarity ($0.50 < D_{min} \leq 0.75$) and MFH with no similarity ($D_{min} > 0.75$). Three samples very similar in gene expression to other sarcoma types ($D_{min} \leq 0.5$) resembled the corresponding histological types of spindle cell and pleomorphic sarcomas, and we concluded that these samples could probably be diagnosed as pleomorphic subtypes of those respective sarcomas based on current histological criteria. We then found that despite only marginal histological resemblance, more than half of the MFH samples (12/21) showed gene expression profiles similar to other sarcoma types ($0.50 < D_{min} \leq 0.75$). We considered that these moderate similarities in gene expression could correspond with pleomorphic change in each sarcoma type. Thus, although the samples cannot be diagnosed based on current histological criteria, it is possible to reclassify them as a pleomorphic subtype of those sarcomas based on gene expression. In this study, 40% (6/15) of reclassified MFH samples ($D_{min} \leq 0.75$) were similar to myxofibrosarcoma and 33% (5/15) were similar to fibrosarcoma, suggesting that a large subset of 'MFH' represents pleomorphic subtypes of fibroblastic sarcomas. Among the six cases of MFH similar to myxofibrosarcoma, five other than NCCS089 had deep-seated lesions, four (NCCS085, NCCS092, NCCS094 and NCCS101) had distant metastasis, and one (NCCS094) suffered local recurrence after surgery. Although the local recurrence rate (1/6) was unexpectedly low and distant metastasis rate (4/6) was high compared to canonical myxofibrosarcoma, these data could be consistent with the report showing that deep-seated lesions of myxofibrosarcoma were higher-grade, pleomorphic and large and increased the incidence of distant metastases.[19] About 30% of the MFH samples (6/21) did not show similarities to other sarcoma types ($D_{min} > 0.75$). One possibility is that '*de novo* undifferentiated pleomorphic sarcomas' truly exist. It is also possible that these samples represent advanced stage of dedifferentiation, which is beyond the analytical power of our study design. Another possibility is that the samples were derived from sarcomas of other differentiation not examined in this study. Extraskeletal osteosarcoma, rhabdomyosarcoma and other sarcomas could be the candidate. Reclassification accuracy should be improved by examining additional histological types of spindle cell and pleomorphic sarcomas.

Given that almost one third of MFH samples shared similar gene expression patterns ($D_{min} \leq 0.75$) with myxofibrosarcoma, we hypothesize that a large subset of 'MFH' may be pleomorphic subtype of myxofibrosarcoma. Myxofibrosarcoma is one of the most frequent sarcomas seen in late adults. However, little is known about its normal tissue counterparts, or factors underlying its extremely high local recurrence rate,[19] nor are there any good markers available for histological diagnosis. Identification of genes highly expressed in myxofibrosarcoma would offer an important clue to address these problems. Here, we found *WISP2*, *GPR64* and *TNXB* were upregulated in myxofibrosarcoma compared with other spindle cell and pleomorphic sarcomas. WISP2 is a member of the WNT1 inducible signaling pathway (WISP) protein subfamily, which belongs to the connective tissue growth factor family. WISP family members are secreted, cell- and matrix-associated proteins that play critical roles in cell differentiation and survival, wound repair, vascular disease, fibrosis and progression of certain cancers.[20–22] GPR64 is a highly conserved, tissue-specific heptahelical receptor of the human epididymis,[23–25] and there are no reports on the relationship of GPR64 to any type of cancer. TNXB is the largest member of the tenascin family of extracellular matrix proteins, which have anti-adhesive effects as opposed to the adhesion activity of fibronectin. It is expressed in musculoskeletal, cardiac and dermis tissue, and its deficiency is associated with the connective tissue disorder Ehlers-Danlos syndrome.[26–28] Although it is not clear if these genes play a role in myxofibrosarcoma, they may serve as novel diagnostic markers.

In this study, we primarily analyzed gene expression of MFH and other types of spindle cell and pleomorphic sarcomas (dedifferentiated liposarcoma, myxofibrosarcoma, leiomyosarcoma, MPNST and fibrosarcoma). Although these sarcomas showed a similar gene expression pattern and formed a relatively loose cluster, samples from five types of spindle cell and pleomorphic sarcomas were classified into respective histological types by excluding MFH samples. We identified genes that were differentially expressed among the five sarcoma types and could reclassify more than 70% of MFH samples into the five sarcoma types based on their similarities in gene expression using a combination of simple statistical analysis. These results suggest that gene expression profiling will be a useful tool to reclassify MFH and to aid histological diagnosis of a diverse group of soft tissue sarcomas. Although we cannot currently predict differences in clinical behavior of reclassified MFH due to the limited number of samples analyzed, accumulation of gene expression data should improve prediction of clinically important events, such as local recurrence, metastasis or therapeutic responses.

Acknowledgement

We are grateful to Ms Rie Ito and Ms Sachiyo Mitani for technical assistance.

Disclosure/conflict of interest

This work was supported by the program for promotion of Fundamental Studies in Health Sciences of the National Institute of Biomedical Innovation (NiBio) and by Grants-in-Aid from the Ministry of Education, Culture, Sports, Science and Technology, Japan. There is no conflict of interest to declare.

References

1 Helman LJ, Meltzer P. Mechanisms of sarcoma development. Nat Rev Cancer 2003;3:685–694.
2 Hasegawa T, Yamamoto S, Nojima T, *et al.* Validity and reproducibility of histologic diagnosis and grading for adult soft-tissue sarcomas. Hum Pathol 2002;33: 111–115.
3 Fletcher CD. Pleomorphic malignant fibrous histiocytoma: fact or fiction? A critical reappraisal based on 159 tumors diagnosed as pleomorphic sarcoma. Am J Surg Pathol 1992;16:213–228.
4 Hollowood K, Fletcher CD. Malignant fibrous histiocytoma: morphologic pattern or pathologic entity? Semin Diagn Pathol 1995;12:210–220.
5 Fletcher CD, Gustafson P, Rydholm A, *et al.* Clinicopathologic re-evaluation of 100 malignant fibrous histiocytomas: prognostic relevance of subclassification. J Clin Oncol 2001;19:3045–3050.
6 Fletcher CD, van den Berg E, Molenaar WM. Pleomorphic malignant fibrous histiocytoma/undifferentiated high grade pleomorphic sarcoma. In: Fletcher CD, Unni KK, Mertens F (eds). World Health Organization Classification of Tumours. Pathology and Genetics of Tumours of Soft Tissue and Bone. IARC Press: Washington, DC, USA, 2002, pp 120–122.
7 Nielsen TO, West RB, Linn SC, *et al.* Molecular characterisation of soft tissue tumours: a gene expression study. Lancet 2002;359:1301–1307.
8 Nagayama S, Katagiri T, Tsunoda T, *et al.* Genome-wide analysis of gene expression in synovial sarcomas using a cDNA microarray. Cancer Res 2002;62:5859–5866.
9 Lee YF, John M, Edwards S, *et al.* Molecular classification of synovial sarcomas, leiomyosarcomas and malignant fibrous histiocytomas by gene expression profiling. Br J Cancer 2003;88:510–515.
10 Segal NH, Pavlidis P, Antonescu CR, *et al.* Classification and subtype prediction of adult soft tissue sarcoma by functional genomics. Am J Pathol 2003; 163:691–700.
11 Skubitz KM, Skubitz AP. Characterization of sarcomas by means of gene expression. J Lab Clin Med 2004; 144:78–91.
12 Baird K, Davis S, Antonescu CR, *et al.* Gene expression profiling of human sarcomas: insights into sarcoma biology. Cancer Res 2005;65:9226–9235.
13 Takahashi H, Nemoto T, Yoshida T, *et al.* Cancer diagnosis marker extraction for soft tissue sarcomas based on gene expression profiling data by using projective adaptive resonance theory (PART) filtering method. BMC Bioinform 2006;7:399.
14 Hasegawa T, Hasegawa F, Hirose T, *et al.* Expression of smooth muscle markers in so called malignant fibrous histiocytomas. J Clin Pathol 2003;56:666–671.
15 Skubitz KM, Cheng EY, Clohisy DR, *et al.* Differential gene expression in liposarcoma, lipoma, and adipose tissue. Cancer Invest 2005;23:105–118.
16 Segal NH, Blachere NE, Guevara-Patino JA, *et al.* Identification of cancer-testis genes expressed by melanoma and soft tissue sarcoma using bioinformatics. Cancer Immun 2005;5:2.
17 Derre J, Lagace R, Nicolas A, *et al.* Leiomyosarcomas and most malignant fibrous histiocytomas share very similar comparative genomic hybridization imbalances: an analysis of a series of 27 leiomyosarcomas. Lab Invest 2001;81:211–221.
18 Coindre JM, Hostein I, Maire G, *et al.* Inflammatory malignant fibrous histiocytomas and dedifferentiated liposarcomas: histological review, genomic profile, and MDM2 and CDK4 status favour a single entity. J Pathol 2004;203:822–830.
19 Mentzel T, Calonje E, Wadden C, *et al.* Myxofibrosarcoma: clinicopathologic analysis of 75 cases with emphasis on the low-grade variant. Am J Surg Pathol 1996;20:391–405.
20 Pennica D, Swanson TA, Welsh JW, *et al.* WISP genes are members of the connective tissue growth factor family that are up-regulated in wnt-1-transformed cells and aberrantly expressed in human colon tumors. Proc Natl Acad Sci USA 1998;95:14717–14722.
21 Brigstock DR. The CCN family: a new stimulus package. J Endocrinol 2003;178:169–175.
22 Perbal B. CCN proteins: multifunctional signalling regulators. Lancet 2004;363:62–64.
23 Kierszenbaum AL. Epididymal G protein-coupled receptor (GPCR): two hats and a two-piece suit tailored at the GPS motif. Mol Reprod Dev 2003;64:1–3.
24 Obermann H, Samalecos A, Osterhoff C, *et al.* HE6, a two-subunit heptahelical receptor associated with apical membranes of efferent and epididymal duct epithelia. Mol Reprod Dev 2003;64:13–26.
25 Kirchhoff C, Obermann H, Behnen M, *et al.* Role of epididymal receptor HE6 in the regulation of sperm microenvironment. Mol Cell Endocrinol 2006;250: 43–48.
26 Burch GH, Gong Y, Liu W, *et al.* Tenascin-X deficiency is associated with Ehlers-Danlos syndrome. Nat Genet 1997;17:104–108.
27 Schalkwijk J, Zweers MC, Steijlen PM, *et al.* A recessive form of the Ehlers-Danlos syndrome caused by tenascin-X deficiency. N Engl J Med 2001; 345:1167–1175.
28 Mao JR, Taylor G, Dean WB, *et al.* Tenascin-X deficiency mimics Ehlers-Danlos syndrome in mice through alteration of collagen deposition. Nat Genet 2002;30:421–425.

Supplementary Information accompanies the paper on Modern Pathology website (http://www.nature.com/modpathol)

J Cancer Res Clin Oncol (2007) 133:697–703
DOI 10.1007/s00432-006-0190-9

ORIGINAL PAPER

New approach for assessing vascular distribution within bone tumors using dynamic contrast-enhanced MRI

Yukio Kawakami · Toshiyuki Kunisada · Shinsuke Sugihara · Atsushi Ono · Keiichiro Nishida · Nobuhiro Abe · Akira Kawai · Kazuo Fujiwara · Yuki Morimoto · Toshifumi Ozaki

Received: 15 September 2006 / Accepted: 11 December 2006 / Published online: 30 May 2007

Abstract
Purpose To differentiate benign from malignant bone tumors by analyzing the vascular distribution within bone tumors with dynamic contrast-enhanced MRI.
Methods We studied dynamic contrast-enhanced MRI for 49 bone tumors (22 malignant and 27 benign tumors). Seven small regions of interest (ROI) were set inside the largest portion of each tumor. Four ROI were placed evenly on the periphery and three ROI were placed evenly on the line of the longest breadth within the tumor. The slope of the curve (%Slope) was calculated on the time–intensity curves of the whole tumor and of each ROI. The variance values for the %Slope of the ROI were calculated to assess the dispersion of the intensity change at each ROI within the tumor.
Results Mean value of the %Slopes of whole tumor regions for malignant bone tumors (70.4 ± 60.3%) was significantly higher than that for benign bone tumors (37.6 ± 52.9%) ($P = 0.015$), although giant cell tumor (GCT), a locally aggressive tumor, had a relatively higher %Slope. Mean value of the variance of %Slopes for malignant bone tumors (3485.9 ± 5942.5) was significantly higher than that for all benign tumors (470.4 ± 583.9) ($P = 0.012$), indicating that the %Slope values of seven ROI within malignant bone tumors varied more widely compared with the ROI inside benign bone tumors. GCT also demonstrated a lower value.
Conclusion Our method of analyzing the signal intensity change at seven separate regions that evaluates the vascular distribution within a tumor could be a useful tool for differentiating between benign and malignant bone tumors.

Keywords Bone tumors · Dynamic contrast-enhanced MRI · Differential diagnosis

Introduction

Magnetic resonance imaging (MRI) has an important role in the diagnosis and management of patients with bone tumors (Zimmer et al. 1985; Pettersson et al. 1987; Bloem et al. 1988; Hoffer et al. 2000). MRI directly demonstrates a lesion relative to the surrounding normal structures with accurate anatomical detail. Although various reports have been designed to characterize bone tumors through MRI, results have been controversial (Lang et al. 1998). The ability of static clinical MRI to depict tumor viability is limited by several factors: (1) T1-weighted MRI alone cannot differentiate viable tumor from non-viable tissue or edema (Holscher et al. 1990), (2) T2-weighted MRI cannot adequately distinguish tumor from necrosis, and lesion boundaries are frequently overestimated because of the presence of edema and hemorrhage (Pan et al. 1990; Sanchez et al. 1990; Brisse et al. 2004), and (3) static

Y. Kawakami · T. Kunisada (✉) · S. Sugihara · K. Nishida · N. Abe · K. Fujiwara · Y. Morimoto · T. Ozaki
Department of Orthopaedic Surgery,
Science of Functional Recovery and Reconstruction,
Okayama University Graduate School of Medicine,
Dentistry and Pharmaceutical Sciences,
2-5-1 Shikata-cho, Okayama 700-8558, Japan
e-mail: toshi-kunisada@umin.ac.jp

A. Ono
Department of Medical Technology,
Okayama Kousei Hospital, Okayama, Japan

A. Kawai
Division of Orthopaedic Surgery,
National Cancer Center Hospital, Tokyo, Japan

T1-weighted contrast media-enhanced MRI can differentiate necrosis and hemorrhage from viable tumor but has difficulty separating viable tumor from surrounding inflammation (Erlemann et al. 1990; Verstraete and Lang 2000).

Dynamic contrast-enhanced MRI is a method of physiologic imaging that evaluates the early enhancement kinetics of water-soluble MR contrast media and shows the signal intensity of a region in real time (Erlemann et al. 1989). Faster contrast enhancement is suitable for visualizing increased vascularity such as capillary permeability and viable tumor, whereas slower enhancement demonstrates less vascular areas such as non-viable tumor, tissue necrosis and inflammation (Kormano and Dean 1976; Verstraete et al. 1995). Dynamic contrast-enhanced MRI is expected to be excellent for assessing response to chemotherapy compared with conventional static MRI because it can assess tumor vascularity that may indicate viability of malignant bone tumors (Erlemann et al. 1990; Fletcher et al. 1992; Kawai et al. 1997; Egmont-Petersen et al. 2000). Despite its usefulness for assessing the therapeutic effect on bone sarcomas, it is still controversial as to whether dynamic contrast-enhanced MRI can differentiate malignant bone tumors from benign bone tumors.

Previous papers demonstrated that the time-course change of intensity can suggest the malignancy of bone tumors with a 60–80% sensitivity (Verstraete et al. 1994b; Bloem et al. 1997; Geirnaerdt et al. 2000). This may be the reason why these papers set the region of interest (ROI) over the entire tumor area imaged in order to examine the intensity change. There are various tissues and fluids within malignant bone tumors, such as high-grade tumor tissue, necrotic and edematous tissue, hemorrhage, and inflammation. One ROI set covering the entire area of a tumor may not be appropriate for evaluating vascularity within a tumor since the intensity change over the whole tumor can be averaged. For studying vascularity of bone tumors, it would be more reliable to designate several ROI sets inside the tumor as seen on MRI and to evaluate each of them. In the present study, we examined the intensity change of seven ROI sets within the tumor boundaries as determined with dynamic MRI and assessed their values for differentiating the malignancy of bone tumors.

Patients and methods

Patients

Forty-nine patients with primary bone tumors were studied using dynamic contrast-enhanced MRI during the preoperative routine examination before initial treatment (Table 1). Diagnosis of all patients was made by histological examination. The patients consisted of 32 males and 17 females with a mean age of 30 years (4–74 years). Twenty-four tumors were of the femur, seven of the tibia, four of the humerus, three of the pelvis, two of the fibula, and nine were from other locations. There were 22 malignant bone tumors, consisting of 15 osteosarcoma, 3 chondrosarcoma, 2 Ewing's sarcoma, 1 malignant fibrous histiocytoma (MFH) and 1 cordoma. There were also 27 benign bone tumors consisting of 5 giant cell tumors (GCT), 5 enchondroma, 4 chondroblastoma, 2 osteochondroma, 2 non ossifying fibroma, 2 aneurysmal bone cysts, 2 eosinophilic granuloma, 2 fibrous dysplasia, 2 solitary bone cysts and 1 osteofibrous dysplasia.

Dynamic contrast-enhanced MRI study

All MR examinations were performed using a 0.5 T (Flexart Hyper; Toshiba, Tokyo, Japan) clinical imager. A quadrature detection (QD) body coil was used for pelvic and femoral imaging, and a 20 cm circular surface coil was adapted for imaging the other locations.

Prior to dynamic contrast-enhanced MRI study, we performed the following pulse sequences: axial, coronal, and sagital T1-weighted spin echo imaging: repetition time (TR), 550 ms; echo time (TE), 15 ms; number of excitations (NEX), 1.7; slice thickness, 5–10 mm, field of view (FOV), 20–35 cm; matrix size, 192 × 256; acquisition time, 6 min, axial, coronal, and sagital T2-weighted fast spin echo imaging: TR, 4,000 ms; TE, 102 ms; echo train length, 13; NEX, 3; slice thickness, 5–10 mm; FOV, 20–35 cm; matrix size, 192 × 256; acquisition time, 6 min 4 s.

For a dynamic contrast-enhanced MRI, imaging plane was selected based on obtaining the largest and most representative area of the tumor. Immediately after the first

Table 1 Pathological diagnosis in 49 patients with bone tumors

Benign tumor	No. (n = 27)	Malignant tumor	No. (n = 22)
Giant cell tumor	5	Osteosarcoma	15
Enchondroma	5	Chondrosarcoma	3
Chondroblastoma	4	Ewing sarcoma	2
Osteochondroma	2	Malignant fibrous histiocytoma	1
Non-ossifying fibroma	2	Chordoma	1
Aneurysmal bone cyst	2		
Eosinophilic granuloma	2		
Fibrous dysplasia	2		
Solitary bone cyst	2		
Osteofibrous dysplasia	1		

sequence, a bolus injection of gadolinium diethylene triamine pentaacetic acid (Gd-DTPA) (0.1 mmol/kg) was administered intravenously followed by ultra-fast sequences using a field echo sequence (TR, 70 ms; TE, 5 ms; flip angle, 70°; NEX, 1; slice thickness, 10 mm; FOV, 20–35 cm; matrix size, 128–192 × 256; echo delay time, 20 ms) at intervals of 13 s for 5 min. The signal intensity of the largest portion of the tumor was measured and plotted against time. The progression of enhancement was subjectively classified into three groups according to the shape of the time–signal intensity curve by modified classification reported previously (van der Woude et al. 1998b) and described in Fig. 1. In the analysis of dynamic MRI, we hypothesized that Type I (rapid pattern) was indicative of malignant lesions, and type II (slow pattern) and type III (flat pattern) were indicative of benign lesions.

Seven regions of interest (ROI) were set within the largest portion of the tumor. Four ROI were placed evenly on the periphery of the largest portion of the tumor, and three ROI were placed evenly on the line of the longest breadth within the tumor (Fig. 2). The signal intensity of each of the seven ROI set inside the tumor were also plotted against time on the time–intensity curve.

The slope of the curve (%Slope), which shows the percent increase in signal intensity per minute over the baseline value, was derived by using the following formula (Erlemann et al. 1990; Hanna et al. 1992) (Fig. 3):

$$\%\mathrm{Slope} = (\mathrm{SI}_{\max} - \mathrm{SI}_{\mathrm{base}}) \times 100/\{\mathrm{SI}_{\mathrm{base}} \times (T_{\max} - T_{\mathrm{base}})\}$$

$\mathrm{SI}_{\max}$: signal intensity demonstrated at a timepoint of $T_{\max}$,
$\mathrm{SI}_{\mathrm{base}}$: signal intensity before the injection of Gd-DTPA,
$T_{\max}$: first timepoint at which the sum of the next two consecutive %Slope values becomes less than 10% per minute,
T_{base}: timepoint immediately preceding signal intensity increase.

The variance values for %Slope of the seven ROI set inside the tumor were calculated to assess the dispersion of the intensity change at each of these ROI, which could indicate the heterogeneity of the vascularity within the tumor.

Statistical analysis

The Mann–Whitney U test was used to evaluate the difference in %Slope and the variance value for %Slope. The

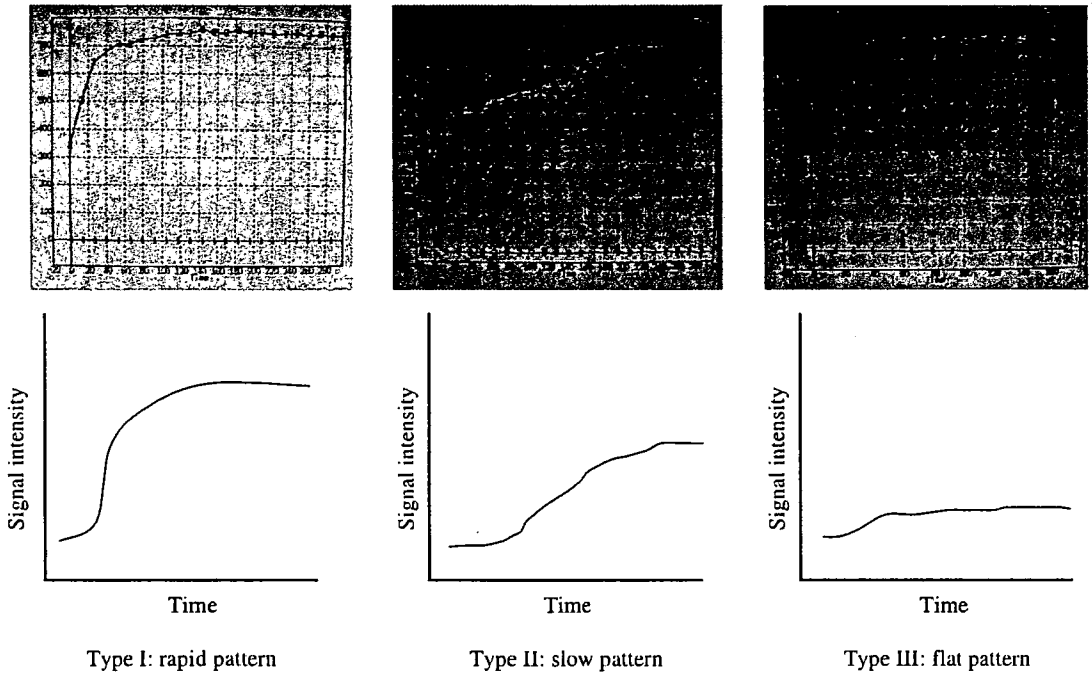

Fig. 1 Three types of time-signal intensity curves reported by van der Woude et al. (1998b). Type I curve (*rapid pattern*): early onset of enhancement followed by rapidly progressive linear increase of signal intensity (represented by a steep slope, parallel to the arterial curve) to an early maximum followed by a distinct transition to a stable level of signal intensity. Type II curve (*slow pattern*): steady increase or flattening of the curve after the steepest part of the time-signal intensity curve. Type III curve (*flat pattern*): linear enhancement with a very low slope, representing slow or absent enhancement, similar to a curve representing normal muscle. In the analysis of dynamic MRI, we hypothesized that Type I curve was indicative of malignant lesions, and Type II and III curves were indicative of benign lesions

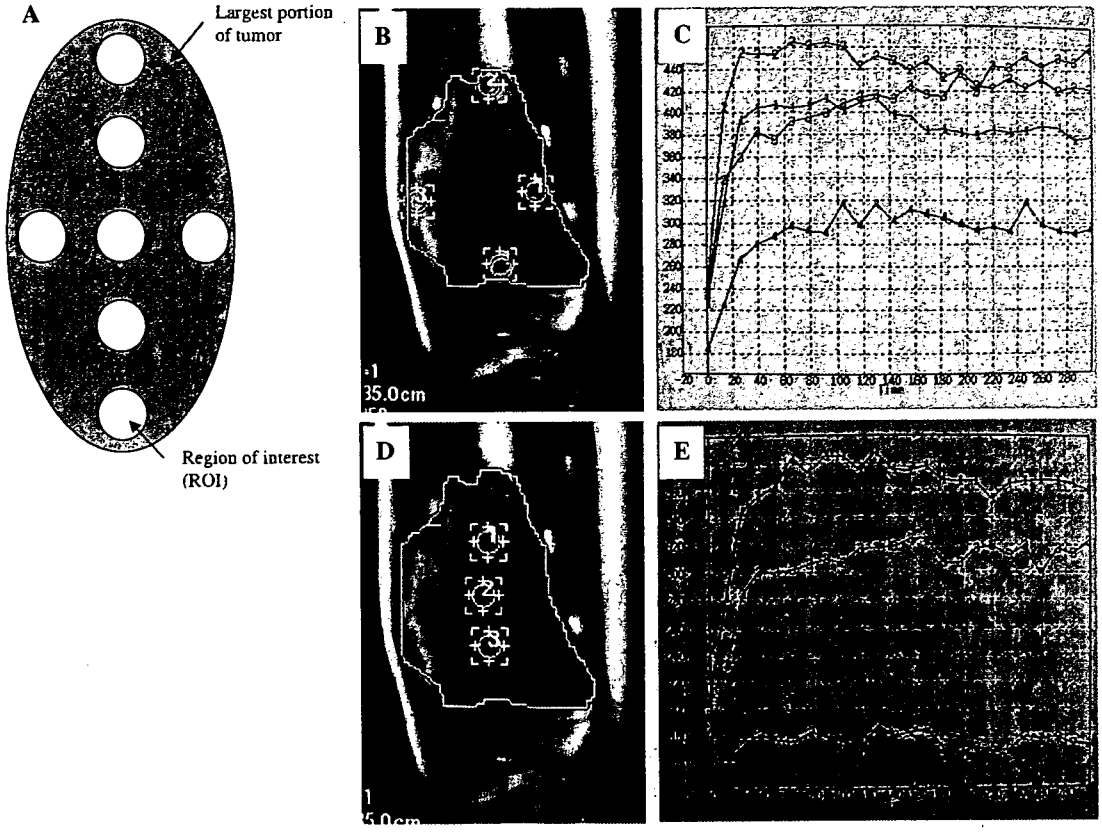

Fig. 2 A large ROI and seven small ROI are set within the largest portion of the tumor (**a**: scheme of 7 ROI set within the tumor). Seven ROI placed on the dynamic contrast-enhanced MRI of osteosarcoma arising from the distal femur (**b, d**). Four ROI were placed evenly on the periphery of the largest portion of the tumor (**b**), and 3 ROI were placed evenly on the line of the longest breadth within the tumor (**d**). The time–signal intensity curves of each 7 ROI were plotted against time on the time–intensity curve (**c, e**)

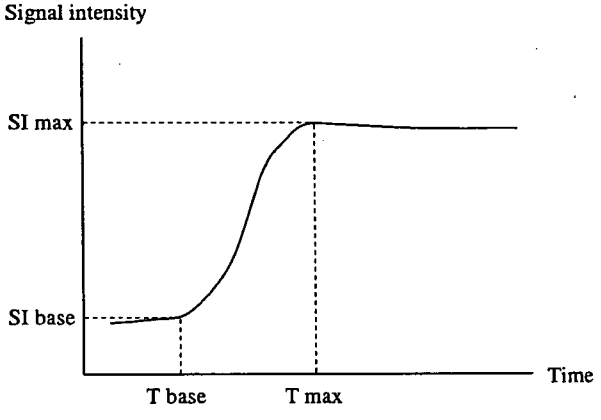

Fig. 3 %Slope was calculated to show the percent increase in signal intensity per minute over the baseline value: $\%Slope = (SI_{max} - SI_{base}) \times 100/\{SI_{base} \times (T_{max} - T_{base})\}$

level of significance was chosen at $P < 0.05$. All data was calculated and evaluated using Statview 5.0J software (SAS Institute Inc., Cary, NC, USA).

Results

Seventeen of 22 malignant bone tumors and 6 of 27 benign bone tumors resulted in the Type I pattern (Table 2). Those 6 benign tumors with Type I pattern consisted of four GCT and two chondroblastoma. Type II pattern was found in 17 benign bone tumors and 4 of 22 malignant bone tumors, which included 2 osteosarcoma and 2 chondrosarcoma. There were four benign bone tumors and one chordoma demonstrating the Type III pattern. Seventeen of 22 malignant bone tumors revealed rapid pattern (Type I curve), and 21 of 27 benign bone tumors demonstrated slow or flat pattern (Type II or III curve). Differentiation of benign from malignant bone tumors based on the time–intensity curve was possible with a sensitivity of 77% and a specificity of 78%.

Table 3 demonstrates each %Slope value representing a whole tumor area with dynamic contrast-enhanced MRI. The mean value of %Slopes for malignant bone tumors (70.4 ± 60.3%) was significantly higher than that for benign bone tumors (37.6 ± 52.9%) ($P = 0.015$, Mann–

Table 2 The pattern of the progression of enhancement on dynamic MRI

Pattern	Benign (n = 27)	Malignant (n = 22)
Type I: rapid pattern	6	17
Type II: slow pattern	17	4
Type III: flat pattern	4	1

Whitney U test). Moreover, this significant difference was even more pronounced (15.8 ± 14.3%) ($P < 0.0001$) when the mean value of %Slopes for GCT (133.4 ± 4.7%) was not counted among the benign bone tumors since the %Slopes for GCT was comparatively higher than the other benign bone tumors. Chordoma, one of the malignant bone tumors, had a lower mean value of %Slope than most of benign tumors.

The variance values for %Slopes of the seven ROI located within a tumor were estimated as the dispersion of intensity change (%Slope) at each ROI of a tumor. Table 4 shows each variance value for the %Slopes of the seven ROI within each tumor. The mean value of the variance of %Slopes for malignant bone tumors (3485.9 ± 5942.5) was significantly higher than that for all benign tumors (470.4 ± 583.9) ($P = 0.012$), indicating that %Slope values of the seven ROIs inside a malignant bone tumor varied more widely than the seven ROI within a benign bone tumor. The vascularity of malignant bone tumors was more heterogeneous than that of benign bone tumors. In particular, the mean variance value of %Slope for GCT (1223.7 ± 727.4) was lower than that of high-grade malignant bone tumors such as MFH (4481.4), osteosarcoma (3953.2 ± 6979.6), and Ewing sarcoma (2720.4 ± 1813.9), indicating that the vascularity within a high-grade malignant tumor is more heterogeneous than that of a GCT. Chordoma had the lowest mean value of the variance of %Slope (0.0) among all the bone tumors.

Table 3 %Slope of the whole tumor area at the largest portion

Malignant tumor	Mean %Slope	Benign tumor	Mean %Slope
Ewing sarcoma	113.1	Giant cell tumor	133.4
Malignant fibrous histiocytoma	82.4	Chondroblastoma	32.8
Osteosarcoma	73.6	Fibrous dysplasia	23.0
Chondrosarcoma	43.3	Eosinophilic granuloma	21.1
Chordoma	7.4	Solitary bone cyst	16.9
		Non-ossifying fibroma	15.9
		Aneurysmal bone cyst	13.0
		Enchondroma	5.7
		Osteofibrous dysplasia	0.0
Average	70.4		37.6

Table 4 The variance value for %Slope of 7ROI located inside the tumor

Malignant tumor	Mean variance value for %Slope	Benign tumor	Mean variance value for %Slope
Malignant fibrous histiocytoma	4481.4	Giant cell tumor	1223.7
Osteosarcoma	3953.2	Aneurysmal bone cyst	726.5
Ewing sarcoma	2720.4	Solitary bone cyst	570.7
Chondrosarcoma	2490.1	Chondroblastoma	523.1
Chordoma	0.0	Non-ossifying fibroma	456.9
		Enchondroma	125.6
		Eosinophilic granuloma	95.7
		Fibrous dysplasia	52.6
		Osteofibrous dysplasia	0.0
Average	3485.9		470.4

Discussion

Dynamic contrast-enhanced MRI, which is performed by ultra fast MRI after a bolus injection of contrast media, can be used to evaluate blood flow by calculating the signal intensity of a region in real time (Erlemann 1992), thus indicating the vascularity of a tumor. By analyzing tumor vascularity using dynamic MRI, many authors have shown that the slope value can be useful for indicating bone tumor viability and predicting tumor necrosis in bone sarcomas after chemotherapy (Erlemann et al. 1990; Bonnerot et al. 1992; Fletcher et al. 1992). Moreover, dynamic contrast-enhanced MRI is excellent for depicting anatomical position like a conventional static MRI and has merit in the evaluation of vascularity in an arbitrary section demonstrating the most representative area of the tumor (Lang et al. 1995; Verstraete and Lang 2000).

van der Woude et al. (1998a) performed dynamic enhanced MRI in 175 patients with a musculoskeletal tumor and assessed the interval between arterial enhancement and onset of tumor enhancement, the pattern (peripheral or diffuse) of initial enhancement, and the shape of the time–signal intensity curve. They concluded that benign bone tumors could not be accurately differentiated from malignant bone tumors on the basis of their defined parameters (sensitivity, 63–76%; specificity, 50–76%). Our study also showed that it was possible, with a sensitivity of 77% and specificity of 78%, to differentiate benign from malignant bone tumors based on the time–intensity curve at one section of a tumor. Bloem et al. (1997) have reported in a

review article concerning MRI for patients with musculoskeletal tumors that not only viable malignant tumors, but also biologically active benign lesions such as eosinophilic granuloma, osteoid osteoma, osteoblastoma, chondroblastoma and GCT displayed rapid-enhancement time–intensity curves of dynamic contrast-enhanced MRI. Furthermore, they reported that not only most benign lesions, but also low-grade chondrosarcoma and sclerotic osteosarcoma, displayed low-enhancement time–intensity curves. We obtained similar results in our series.

Our results demonstrated that the mean value of the %Slopes for malignant bone tumors (70.4 ± 60.3%) was significantly higher than that for benign bone tumors (37.6 ± 52.9%). Verstraete et al. (1994b) reported that a significant difference was found in the slope values of dynamic contrast-enhanced MRI between malignant and benign musculoskeletal tumors. However, they indicated that dynamic contrast-enhanced MRI could depict tissue vascularization and perfusion rather than actual benignity or malignancy since there was an overlap in the slope values of highly vascular benign lesions and malignant lesions.

GCT, the most common benign tumor in our series, had the highest mean value of %Slope (133.4) among all the bone tumors. Verstraete et al. (1994a) also demonstrated same result that GCT showed the highest mean value of %Slope among all musculoskeletal tumors. Chordoma, one of low-grade malignant bone tumors, had much lower mean value of %Slope (7.4) than the average of benign bone tumors (37.6). van der Woude et al. (1998b) showed that only 6 of 26 low-grade malignant tumors showed a Type I curve. There was also a considerable overlap of %Slope value between aggressive benign bone tumors and low-grade malignant tumors.

As mentioned above, the overall rate of enhancement is not a reliable indicator of a benign versus a malignant bone lesion. As a method for evaluating any difference in enhancement within a tumor, Ma et al. have reported that the rim-to-center differential enhancement ratio can potentially be used to differentiate benign from malignant bone tumors (Ma et al. 1997). The increased rim enhancement with delayed center enhancement, which indicated a solid, malignant mass of bone, might be due, in part, to the high internal, interstitial pressure exhibited by malignant neoplasms but not benign tumors. There are generally some necrotic areas and/or undifferentiated lesions with aggressive tumor tissue inside a malignant tumor mass, indicating that the inside of a malignant tumor can be vascularly heterogeneous. The rim-to-center enhancement cannot be enough to reflect the vascular heterogeneity inside the tumor.

In order to study the vascular heterogeneity inside a tumor, we set up seven small ROI within each tumor and calculated the intensity change of each ROI. We considered the variance value for slopes of the seven ROI as the dispersion of the blood flow at each ROI, which demonstrated the heterogeneity of vascularity inside the tumor. The distribution of slope values in malignant bone tumors was significantly higher than that in benign tumors. This suggested that the malignant bone tumors were composed of regions having various changes of signal intensity, indicating that the viability inside malignant tumors was heterogeneous. Therefore, seven ROI could also be useful for determining the optimum site for biopsy.

Chordoma, one of low-grade malignant tumors, had the lowest mean value of the variance of %Slopes among all the bone tumors in the present study. This might be the reason why chordoma was only one case in our series and showed very low vascularity within the tumor. Because the number of each tumor type is small (n = 1–5), except for osteosarcoma (n = 15) in the present study, prospective studies that include larger numbers of patients are needed to validate the use of our analyzing method.

In conclusion, the signal intensity change observed with dynamic contrast-enhanced MRI can be used to assess the vascularity of a tumor. Previous papers showed that the intensity change over a whole tumor section can predict the viability of the tumor, but this method was not enough to determine the malignancy of bone tumors. Our method of analysis looking at the intensity change at seven separate regions can indicate the heterogeneity of vascularity within a tumor, which could make our method useful for differentiating between benign and malignant bone tumors.

Acknowledgments This work was supported in part by a Grant-in-aid for Young Scientists (B) from the Ministry of Education, Culture, Sports, Science and Technology (No.18791040, No.15790792), by a grant from Japan Orthopaedics and Traumatology Foundation Inc. (No.0158), by Grants-in-Aid for Clinical Cancer Research and Grants-in-Aid for Cancer Research (14S-4 and -5) from the Ministry of Health, Labor and Welfare, and by a grant from JSPS Fujita Memorial Fund for Medical Research.

References

Bloem JL, Taminiau AH, Eulderink F, Hermans J, Pauwels EK (1988) Radiologic staging of primary bone sarcoma: MR imaging, scintigraphy, angiography, and CT correlated with pathologic examination. Radiology 169:805–810

Bloem JL, van der Woude HJ, Geirnaerdt M, Hogendoorn PC, Taminiau AH, Hermans J (1997) Does magnetic resonance imaging make a difference for patients with musculoskeletal sarcoma? Br J Radiol 70:327–337

Bonnerot V, Charpentier A, Frouin F, Kalifa C, Vanel D, Di Paola R (1992) Factor analysis of dynamic magnetic resonance imaging in predicting the response of osteosarcoma to chemotherapy. Invest Radiol 27:847–855

Brisse H, Ollivier L, Edeline V, Pacquement H, Michon J, Glorion C, Neuenschwander S (2004) Imaging of malignant tumours of the long bones in children: monitoring response to neoadjuvant

chemotherapy and preoperative assessment. Pediatr Radiol 34:595–605

Egmont-Petersen M, Hogendoorn PC, van der Geest RJ, Vrooman HA, van der Woude H, Janssen JP, Bloem JL, Reiber JH (2000) Detection of areas with viable remnant tumor in postchemotherapy patients with Ewing's sarcoma by dynamic contrast-enhanced MRI using pharmacokinetic modeling. Magn Reson Imaging 18:525–535

Erlemann RP (1992) Dynamic Gd-DTPA-enhanced MR imaging in the musculoskeletal system. In: Higgins HH, Helms C (eds) Magnetic resonance imaging of the body. Raven Press Ltd., New York

Erlemann R, Reiser MF, Peters PE, Vasallo P, Nommensen B, Kusnierz-Glaz CR, Ritter J, Roessner A (1989) Musculoskeletal neoplasms: static and dynamic Gd-DTPA-enhanced MR imaging. Radiology 171:767–773

Erlemann R, Sciuk J, Bosse A, Ritter J, Kusnierz-Glaz CR, Peters PE, Wuisman P (1990) Response of osteosarcoma and Ewing sarcoma to preoperative chemotherapy: assessment with dynamic and static MR imaging and skeletal scintigraphy. Radiology 175:791–796

Fletcher BD, Hanna SL, Fairclough DL, Gronemeyer SA (1992) Pediatric musculoskeletal tumors: use of dynamic, contrast-enhanced MR imaging to monitor response to chemotherapy. Radiology 184:243–248

Geirnaerdt MJ, Hogendoorn PC, Bloem JL, Taminiau AH, van der Woude HJ (2000) Cartilaginous tumors: fast contrast-enhanced MR imaging. Radiology 214:539–546

Hanna SL, Parham DM, Fairclough DL, Meyer WH, Le AH, Fletcher BD (1992) Assessment of osteosarcoma response to preoperative chemotherapy using dynamic FLASH gadolinium-DTPA-enhanced magnetic resonance mapping. Invest Radiol 27:367–373

Hoffer FA, Nikanorov AY, Reddick WE, Bodner SM, Xiong X, Jones-Wallace D, Gronemeyer SA, Rao BN, Kauffman WM, Laor T (2000) Accuracy of MR imaging for detecting epiphyseal extension of osteosarcoma. Pediatr Radiol 30:289–298

Holscher HC, Bloem JL, Nooy MA, Taminiau AH, Eulderink F, Hermans J (1990) The value of MR imaging in monitoring the effect of chemotherapy on bone sarcomas. AJR Am J Roentgenol 154:763–769

Kawai A, Sugihara S, Kunisada T, Uchida Y, Inoue H (1997) Imaging assessment of the response of bone tumors to preoperative chemotherapy. Clin Orthop 337:216–225

Kormano M, Dean PB (1976) Extravascular contrast material: the major component of contrast enhancement. Radiology 121:379–382

Lang P, Honda G, Roberts T, Vahlensieck M, Johnston JO, Rosenau W, Mathur A, Peterfy C, Gooding CA, Genant HK (1995) Musculoskeletal neoplasm: perineoplastic edema versus tumor on dynamic postcontrast MR images with spatial mapping of instantaneous enhancement rates. Radiology 197:831–839

Lang P, Johnston JO, Arenal-Romero F, Gooding CA (1998) Advances in MR imaging of pediatric musculoskeletal neoplasms. Magn Reson Imaging Clin N Am 6:579–604

Ma LD, Frassica FJ, McCarthy EF, Bluemke DA, Zerhouni EA (1997) Benign and malignant musculoskeletal masses: MR imaging differentiation with rim-to-center differential enhancement ratios. Radiology 202:739–744

Pan G, Raymond AK, Carrasco CH, Wallace S, Kim EE, Shirkhoda A, Jaffe N, Murray JA, Benjamin RS (1990) Osteosarcoma: MR imaging after preoperative chemotherapy. Radiology 174:517–526

Pettersson H, Gillespy T III, Hamlin DJ, Enneking WF, Springfield DS, Andrew ER, Spanier S, Slone R (1987) Primary musculoskeletal tumors: examination with MR imaging compared with conventional modalities. Radiology 164:237–241

Sanchez RB, Quinn SF, Walling A, Estrada J, Greenberg H (1990) Musculoskeletal neoplasms after intraarterial chemotherapy: correlation of MR images with pathologic specimens. Radiology 174:237–240

van der Woude HJ, Bloem JL, Hogendoorn PC (1998a) Preoperative evaluation and monitoring chemotherapy in patients with high-grade osteogenic and Ewing's sarcoma: review of current imaging modalities. Skeletal Radiol 27:57–71

van der Woude HJ, Verstraete KL, Hogendoorn PC, Taminiau AH, Hermans J, Bloem JL (1998b) Musculoskeletal tumors: does fast dynamic contrast-enhanced subtraction MR imaging contribute to the characterization? Radiology 208:821–828

Verstraete KL, Lang P (2000) Bone and soft tissue tumors: the role of contrast agents for MR imaging. Eur J Radiol 34:229–246

Verstraete KL, De Deene Y, Roels H, Dierick A, Uyttendaele D, Kunnen M (1994a) Benign and malignant musculoskeletal lesions: dynamic contrast-enhanced MR imaging-parametric "first-pass" images depict tissue vascularization and perfusion. Radiology 192:835–843

Verstraete KL, Dierick A, De Deene Y, Uyttendaele D, Vandamme F, Roels H, Kunnen M (1994b) First-pass images of musculoskeletal lesions: a new and useful diagnostic application of dynamic contrast-enhanced MRI. Magn Reson Imaging 12:687–702

Verstraete KL, Vanzieleghem B, De Deene Y, Palmans H, De Greef D, Kristoffersen DT, Uyttendaele D, Roels H, Hamers J, Kunnen M (1995) Static, dynamic and first-pass MR imaging of musculoskeletal lesions using gadodiamide injection. Acta Radiol 36:27–36

Zimmer WD, Berquist TH, McLeod RA, Sim FH, Pritchard DJ, Shives TC, Wold LE, May GR (1985) Bone tumors: magnetic resonance imaging versus computed tomography. Radiology 155:709–718

Jpn J Clin Oncol 2007;37(12)955–960
doi:10.1093/jjco/hym125

Prognostic Implications of Glucose Transporter Protein-1 (Glut-1) Overexpression in Bone and Soft-Tissue Sarcomas

Makoto Endo[1], Ukihide Tateishi[2], Kunihiko Seki[3], Umio Yamaguchi[1], Fumihiko Nakatani[1], Akira Kawai[1], Hirokazu Chuman[1] and Yasuo Beppu[1]

[1]Division of Orthopaedic Oncology, National Cancer Center Hospital, Tokyo, [2]Division of Diagnostic Radiology, National Cancer Center Hospital, Tokyo, Japan and [3]Division of Clinical Laboratory, National Cancer Center Hospital, Tokyo, Japan

Received June 28, 2007; accepted August 13, 2007

Background: The glucose transporter protein 1 (Glut-1) overexpression is associated with poor overall survival (OS) in various malignant tumors. The aim of this study was to investigate prognostic significance of Glut-1 overexpression in patients with bone and soft-tissue sarcomas.

Methods: A total of 67 patients (mean age, 43 years; range, 8–79 years) with bone and soft tissue sarcomas were analyzed. Pathologic confirmation was observed from surgical specimens in all patients. Pathologic variables including tumor differentiation, necrosis, mitotic index, MIB-1 (Ki-67) grade and Glut-1 expression were assessed. Clinical characteristics and pathologic variables were determined by Kaplan–Meyer curve of OS after treatment.

Results: Glut-1 overexpression was found in 56 patients (83%). The patients with Glut-1 overexpression showed significantly poor OS compared with those without Glut-1 overexpression ($P = 0.029$). The presence of metastasis, treatment without surgical resection, tumor differentiation, necrosis, mitotic index and MIB-1 grade were also significantly negative prognostic factors. The presence of metastasis was independently associated with poor OS ($P = 0.031$).

Conclusions: Assessment of Glut-1 expression prior to treatment has a predictive potential effect in patients with bone and soft-tissue sarcomas.

Key words: sarcoma – glucose trasnsporter protein – prognosis

INTRODUCTION

Bone and soft-tissue sarcomas are classified according to their grade, which represents the most important prognostic factors. The presence of necrosis has been shown to be an independent parameter for predicting prognosis (1). The size and the location of the tumor are other important prognostic factors (2).

The glucose transporter protein-1 (Glut-1) is one of the proteins upregulated in hypoxic conditions. The presence of hypoxia in tumors is leading to resistance to radiotherapy and chemotherapy and is associated with an increased potential for metastases (3–5). This latter finding is thought to be related to the promotion of genomic instability associated with an carcinogenesis and malignant progression (6). Glut-1 is also associated with an increased expression of some proteins that can change tumor cells to survive the severe microenvironment. Glut-1 also promotes glucose metabolism and is overexpressed in several tumors (7–9). The level of Glut-1 expression might be a suitable marker of hypoxia and glucose metabolism, which could be measured simply and inexpensively as part of the routine histologic assessment of tumors (10,11). Increased expression of Glut-1 has been shown to be correlated with a poor prognosis in a variety of tumors (12–14). However, little is known about its expression in bone and soft-tissue sarcomas.

In the present study, immunohistochemical staining of Glut-1 was performed prospectively in the patients with bone and soft-tissue sarcomas. The aim of the present study was to test the hypothesis that Glut-1 overexpression is related to the clinical outcome in patients with bone and soft-tissue sarcomas.

For reprints and all correspondence: Ukihide Tateishi, Division of Diagnostic Radiology, National Cancer Center Hospital, 5-1-1, Tsukiji, Chuo-ku, 104-0045, Tokyo, Japan. E-mail: utateish@ncc.go.jp

PATIENTS AND METHODS

Patients

Sixty-seven patients aged 8–79 years and having histologically proven sarcomas arising from bone ($n = 22$, 33%) or soft tissue ($n = 55$, 67%) since July 2001 until July 2006 were included in this study. All patients underwent initial staging based on a review of the medical history, physical examinations and imaging studies. This study was conducted in accordance with the Helsinki declaration, and all the patients had provided their informed consent for the review of their records.

Treatment and Follow-up

Surgical resection was performed in 54 patients (81%). Surgical procedures were wide resection ($n = 33$, 61%), marginal resection ($n = 15$, 22%), radical resection ($n = 3$, 4%) and intralesional resection ($n = 3$, 4%). Adjuvant chemotherapy was performed in 46 patients (69%). Radiotherapy was performed in 24 patients (36%), mean dose was 46.5 Gy (range, 30–70.4 Gy). The follow-up period was dated from the time of diagnosis, and the mean follow-up period was 25 months (range, 6–60 months). During the follow-up, 39 patients (58%) developed metastases. Metastatic sites included lung ($n = 26$, 39%), bone ($n = 7$, 10%), lymph node ($n = 6$, 9%), soft tissue ($n = 4$, 6%), adrenal gland ($n = 2$, 3%), liver ($n = 1$, 1%), heart ($n = 1$, 1%) and pancreas ($n = 1$, 1%). Seventeen patients (25%) died with disease, 19 patients (28%) were alive with disease and 31 patients (46%) were no evidence of disease.

Histological Examination

Pathology specimens of all the patients' tumors were obtained by incisional biopsy or surgical resection after the imaging studies, and histologic slides were prepared by two expert pathologists for diagnosis. Each tumor was staged according to the TNM classification of UICC and AJCC staging protocol for bone and soft-tissue sarcomas (15,16). Whenever necessary, immunohistochemical staining was carried out to confirm the diagnosis or tumor type according to the WHO classification system (17). The histologic grade of the tumor was determined using a three-grade system in which tumor differentiation, tumor necrosis and MIB-1 LI were given a score of 0, 1, 2 or 3, respectively, and the scores were added together (18). Lesions with MIB-1 LI of 0–9, 10–29 and >30% were assigned MIB-1 scores of 1, 2 and 3, respectively. The three separate scores were added together to produce a combined grade: lesions whose total score was 2 or 3 were classified as Grade 1, those whose total score was 4 or 5 were clarified as Grade 2 and those whose total score was 6, 7 or 8 were clarified as Grade 3. According to this MIB-1 system, tumors were assigned Grades 1–3.

Immunohistochemical Analysis of Glut-1

Immunohistochemical analysis was performed using the labeled streptavidin–biotin method and tissue sections from paraffin blocks. The sections were dewaxed, rehydrated and moistened, then pretreated in an autoclave before being incubated with an affinity-purified goat polyclonal anti-Glut-1 antibody (A3536; diluted 1:500; DakoCytomation). The intensity of Glut-1 staining was quantified with regard to the percentage of cells stained. It was scored as 0 (0%), 1 (1–9%), 2 (10–29%) or 3 (>30%). The results were evaluated by an expert pathologist who was unaware of the clinical status of the patients. The sections were examined using a multi-head microscope, and a consensus judgment was adopted based on Glut-1 staining score of the tumor. The staining scores of 2 and 3 were regarded as indicators of the overexpression of Glut-1.

Statistical Analysis

For the study of the prognostic value, overall survival (OS) was chosen as an end point. OS was defined as the time from diagnosis to death from any cause. Univariate regression analysis was performed to assess the value of all the prognostic factors for the prediction of OS by comparing Kaplan–Meier os curves and carrying out log-rank tests. Kruskal–Wallis test was performed to compare the relations between MIB-1 grade and Glut-1 intensity. Multivariate proportional hazards (Cox) regression analysis was used to test the independency of established prognostic factors for the prediction of OS. Differences and correlations at a P-value of <0.05 was considered statistically significant. All data analyses were performed using SPSS 12.0J (SPSS, Chicago, IL, USA).

RESULTS

The characteristics of 67 patients (mean age, 43 years; range, 8–79 years) are shown in Table 1. Most frequent histologic types were osteosarcoma ($n = 16$, 24%) followed by pleomorphic malignant fibrous histiocytoma ($n = 12$, 18%). The tumors were located in the trunk in 37 patients (55%) and in the extremity in 30 patients (45%). The largest diameter of the tumor is 9.4 cm (range, 1.2–24.0 cm). Twenty-two bone sarcomas (33%) and 45 soft-tissue sarcomas (67%) were also included in Table 1. Tumor stage was IA ($n = 2$, 3%), IB ($n = 4$, 6%), IIA ($n = 14$, 21%), IIB ($n = 9$, 13%), III ($n = 12$, 18%), IV ($n = 18$, 27%), IVA ($n = 4$, 6%) and IVB ($n = 4$, 6%).

The univariate analysis results are summarized in Table 2. The presence of metastasis ($P = 0.0030$) and the treatment without surgical resection ($P = 0.0010$) were significantly associated with poor OS. Age, gender, tumor type, anatomical site (trunk or extremity), tumor size and treatment modality had no prognostic value.

Table 1. Patient characteristics

Parameter	Value (%)
Age (year)	
Mean ± SD	43 ± 22
Median	38
Range	8–79
Gender	
Male	42 (63)
Female	25 (37)
Histologic diagnosis	
Osteosarcoma	16 (24)
Pleomorphic MFH	12 (18)
Liposarcoma	6 (9)
Ewing sarcoma	6 (9)
Chondrosarcoma	5 (7)
Synovial sarcoma	5 (7)
Myxofibrosarcoma	4 (6)
Leiomyosarcoma	3 (4)
Rhabdomyosarcoma	3 (4)
Angiosarcoma	2 (3)
Alveolar soft-tissue sarcoma	1 (1)
Epithelioid sarcoma	1 (1)
Fibrosarcoma	1 (1)
MPNST	1 (1)
Unclassified	1 (1)

The numbers of the parentheses are percentages.
SD, standard deviation; MFH, malignant fibrous histiocytoma; MPNST, malignant peripheral nerve sheath tumor.

Mitotic grades were Grade 1 ($n = 8$, 12%), Grade 2 ($n = 11$, 16%) and Grade 3 ($n = 48$, 72%). The median MIB-1 index of tumor was 32.5%. MIB-1 grades were Grade 1 ($n = 7$, 10%), Grade 2 ($n = 10$, 15%) and Grade 3 ($n = 50$, 75%). On the basis of pathologic examinations, it was found that tumor differentiation ($P = 0.0165$), necrosis ($P = 0.0399$), mitotic index ($P = 0.0071$) and MIB-1 grade ($P = 0.0311$) were associated with a trend toward poor OS.

Glut-1 expression (Figs 1–3) was found in 64 patients (96%) and their intensity was 1 ($n = 8$, 12%), 2 ($n = 15$, 22%) and 3 ($n = 41$, 61%). Glut-1 immunostaining was absent in three tumors (4%): two well-differentiated liposarcomas and one clear cell chondrosarcoma. Along with Glut-1 expression in cytoplasm of tumor cells, specific Glut-1 expression was also seen in erythrocytes, perineurium of the peripheral nerves and lymphocytes in the germinal zone. Glut-1 overexpression was significantly associated with the histologic grade by Kruskal–Wallis test ($P < 0.0001$) (Table 3). No significant difference in Glut-1 staining intensity was found among the other variables, including age, gender, anatomical site (trunk or extremity), tumor size and

Table 2. Univariate analysis of overall survival (OS)

Variables	*n*	1-year survival (%)	2-year survival (%)	3-year survival (%)	*P* value
Age (years)					
<38	33	90.2	81.5	73.4	0.7592
≥38	34	88.0	76.7	68.2	
Gender					
Female	25	95.8	91.5	74.9	0.4413
Male	42	85.0	69.9	69.9	
Tumor type					
Bone sarcoma	22	90.4	90.4	81.4	0.8504
Soft-tissue sarcoma	45	88.5	73.5	65.4	
Anatomical site					
Extremities	30	92.7	81.8	81.8	0.1316
Trunk	37	86.2	76.8	59.7	
Metastasis					
Negative	28	96.4	96.4	96.4	0.0030
Positive	39	84.3	68.2	57.2	
Size (cm)					
0–5	16	100.0	100.0	100.0	0.0506
5–10	22	80.0	56.3	42.2	
>10	29	89.7	80.4	71.5	
SR					
(−)	13	61.5	52.8	52.8	0.0010
(+)	54	96.0	86.1	76.8	
AC					
(−)	20	89.7	89.7	89.7	0.0740
(+)	47	88.9	75.1	63.0	
RT					
(−)	43	90.3	87.5	81.3	0.0909
(+)	24	87.1	67.0	53.6	
Therapeutic combination					
AC alone	5	40.0	40.0	40.0	<0.0001
RT alone	1	0.0	0.0	0.0	
AC + RT	7	85.7	68.6	68.6	
SR alone	17	100.0	100.0	100.0	
SR + AC	22	94.4	87.7	73.1	
SR + AC + RT	15	93.3	70.6	56.6	
Tumor differentiation					
1 or 2	15	100.0	100.0	100.0	0.0165
3	52	85.9	73.8	64.3	
Necrosis					
0	41	92.6	85.4	72.3	0.0399
1	11	90.9	80.8	80.8	
2	15	78.6	62.5	62.5	

Continued